The Magdalena Ridge Observatory Interferometer: custom near-IR beamsplitter and AR coatings

E.K. Block [a*], C.A. Jurgenson [a], D.F. Busher [b], C.A. Haniff [b], J.S. Young [b], M.J. Creech-Eakman [a], A. Jaramillo [c], R. Schmell [c]

[a] New Mexico Institute of Mining and Technology, Magdalena Ridge Observatory, 801 Leroy Place, Socorro, NM 87801, USA;
[b] University of Cambridge, Cavendish Laboratory, Dept. of Physics, JJ Thomson Avenue, Cambridge, CB3 OHE, UK;
[c] Optical Surface Technologies, 2801 Unit E Broadbent Parkway N. E, Albuquerque, NM 87107, USA

ABSTRACT

This report focuses on the design, application, and testing of custom beamsplitter and anti-reflection coatings for use in the Magdalena Ridge Observatory Interferometer (MROI) beam combiners. The coatings were designed in collaboration with Optical Surface Technologies, and the University of Cambridge. The fringe tracker and science combiners will operate across the J, H, and K bands. The coatings were designed to achieve three optical characteristics critical to optical interferometry: 1) minimized stress of the substrate (leading to induced wavefront errors), 2) high throughput, and 3) high visibilities in broadband unpolarized light. The AR coating has mean reflection losses of less than 0.5%. Beamsplitter coatings experienced visibility losses less than 1% due to group delay dispersion and s and p phase differences.

Keywords: MROI, interferometry, beamsplitter, anti-reflection (AR), coatings, pupil plane combination.

1. INTRODUCTION

The Magdalena Ridge Observatory is building an optical/infrared (0.6-2.4 micron) imaging interferometer. The main science goal is to deliver model independent images of faint and complex astronomical targets with milli-arcsecond spatial resolutions. The array will be situated on top of the Magdalena Ridge's South Baldy Peak at an elevation of approximately 3,200 meters and be comprised of 10 x1.4-meter telescopes arranged in a "Y" configuration illustrated in Figure 1. There will be a total of 28 foundation pads which will allow for 4 array configurations of the 10 telescopes. The infrastructure upon completion will have baselines of 7.5 to 340 m[1].

The interferometer will have three beam combiners, two for science (visible and IR) and the third for fringe tracking. The fringe tracker (FT) combiner, illustrated schematically in Figure 1[2], will be dedicated to phasing up the three arms of the array via baseline bootstrapping[3]. The FT combiner is optimized for group-delay fringe tracking allowing for tracking on sources approximately 2.5-magnitudes fainter than are accessible to phase-tracking systems[4]. The tracking will be switchable between the H band (1.4-1.8μm wavelength) and the K_s band (2.0-2.31μm wavelength) to allow simultaneous science operations in any of the three IR bands (J, H, K) without having to share light between the combiners.

*E.K. Block, eblock@mro.nmt.edu, www.mro.nmt.edu

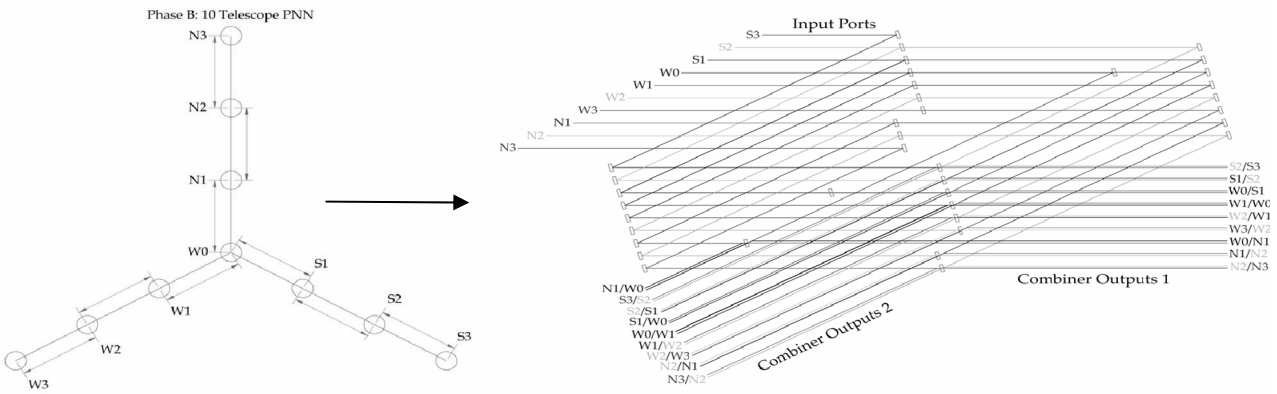

Fig.1. (Left) a 2D schematic showing the MROI array layout with nearest neighbor combinations. The circles represent telescopes designated north (N), south (S), and west (W). The central telescope, W0, has three combination partners: N1, S1, and W1 and is responsible for phasing up the entire array via baseline bootstrapping. (Right) the resultant FT beam combiner layout showing all 10 telescope beams entering at upper left with complimentary outputs at lower left and right. The notation at each output, such as N1/S2, means that the beams from the N1 and S2 telescopes are in that output.

Three custom coatings have been designed and optimized to minimize visibility losses within the beam combiner due to intensity mismatch, polarization, and group delay. The three coatings include: a custom AR coating for both the near-infrared fringe tracking and science instruments and two beamsplitter coatings (50% and 33.33%) for the fringe tracker. The 33.33% beamsplitter coating is to accommodate the three combination partners of the central telescope (one partner from each arm of the array) which will allow for proper phasing up of the entire array. The purpose of this paper is to analyze each coating's design and overall combiner performance.

2. COATING DESIGN

Coating design and analysis was performed using the *Essential Macleod Optical Thin Film Design and Analysis* software package. Each coating was designed with a reference wavelength of 1500nm and at an incident angle of 15 degrees. Infrasil 301(n=1.44473) was chosen as the substrate material for beam combiner optics because of its transparency through the K band unlike other glasses which have significant losses. Infrasil 301 also possesses high homogeneity and absence of striations in all three dimensions (properties very important to multiple axis optics such as beamsplitters). There are three different coatings which will be applied to the Infrasil 301 substrates:

1. Anti-reflection (AR) coating
2. 33.33% reflectance beamsplitter coating
3. 50% reflectance beamsplitter coating

The AR coatings will be applied to both sides of the compensator plates and one side of each beamsplitter plate to minimize internal reflections and achieve high throughput. Only one plate will receive the 33.33% reflective coating; the first beamsplitter encountered by the central telescope, W0. The AR coating is optimized for operation in the J, H, and K bands (1.1 μm to 2.4 μm) allowing it to be used by both the FT and IR science combiners. The beamsplitter coatings, only used in the FT, were optimized for operation in the H and K_s bands only (1.5 μm to 2.31 μm).

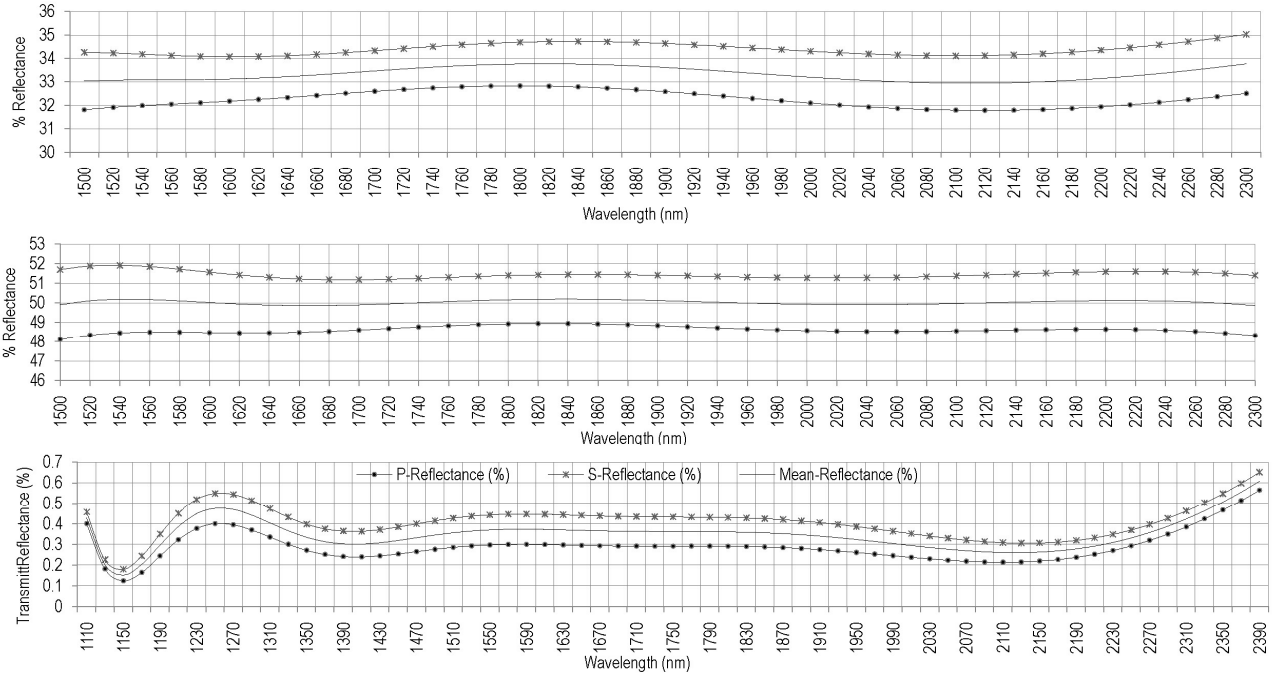

Fig.2. Theoretical performance plots for the, 33.33%, 50%, and AR coatings.

All coatings consist of a top layer of magnesium fluoride (MgF_2) followed by alternating layers of niobium oxide (Nb_2O_5) and silicon dioxide (SiO_2) of varying optical and physical thicknesses. The AR coating is comprised of 14 layers with a total physical thickness of 1432 nm, the 33.33% beamsplitter coating is comprised of 9 layers with a total physical thickness of 1476 nm and the 50% beamsplitter coating is comprised of 8 layers with a total physical thickness of 1847 nm. Figure 2 shows the theoretical performance plots of each coating in terms of s/p polarizations and mean reflectance as a function of wavelength. From these plots it can be seen that the theoretical performance for all three coatings is very good with minimal deviations in reflectance across the optimized wavelengths. The effect of small manufacturing errors was also analyzed in the *Essential Macleod* and confirmed that with reasonable manufacturing imperfections, the coatings will still yield good performance.

Another factor of concern was the bending of the substrate surface during the coating application process. The substrates were fabricated to introduce no more than $\lambda/20$ wavefront error upon transmission or reflection, and this is to be maintained after the application of the coatings. To reduce bending of the substrate, the coating design philosophy was to keep the total number of layers as well as the total thickness to a minimum. In addition, the Infrasil substrates were made thick relative to their diameter. Finally, the coating deposition itself will take place via a low temperature sputtering process.

3. COATING ANALYSIS

3.1 FT combination paths

The performance of the three custom coatings was done by analyzing individual paths through the FT beam combiner. The FT layout is shown in Figure 1 where the light from all 10 unit telescopes (UTs) enter at the upper left and exit after combination at two complementary outputs. Because beams in the combiner traverse various components in different directions and in different orders, there exist different paths (designated A through H) through the combiner which are not all identical in detail. These eight unique paths comprise six non-redundant combination pairs: A-B, C-B, D-E, F-B, C-G, and C-H; Figure 3 shows their differences explicitly. Given the coating properties it is the differences between these paths that need to be analyzed – in particular, how the coating properties and these differences impact the interferometric performance.

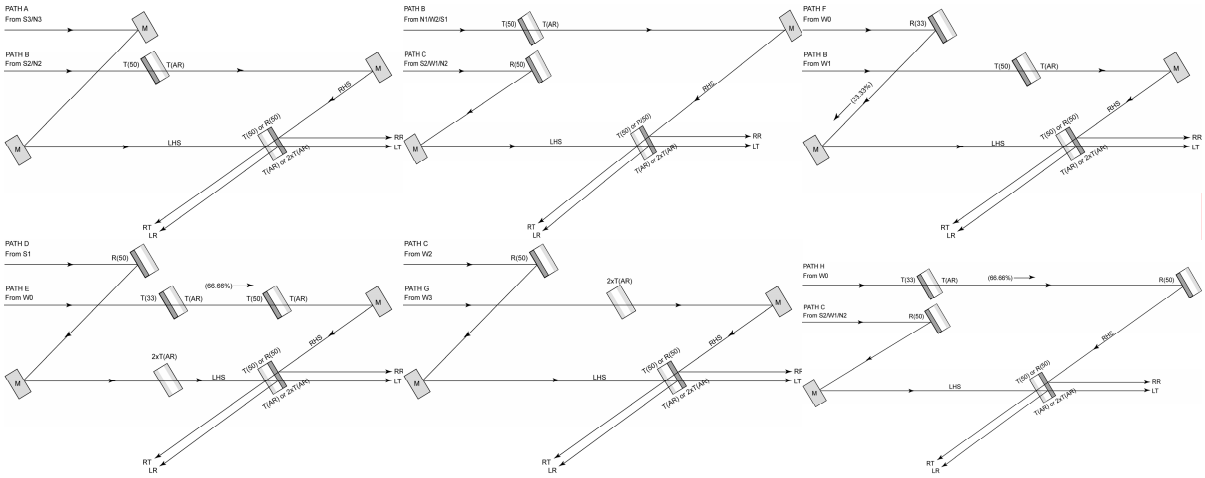

Fig.3. This figure shows the six non-redundant combination through the FT beam combiner resulting from beams in the combiner traversing various components in different directions and in different orders. From top to bottom, path A-B, C-B, F-B, D-E, C-G, and C-H. Optics include: gold mirrors, 33.33% and 50% beamsplitters, and compensator plates. Transmissions (T) and reflections (R) are labeled. The AR coating will be applied to one side of each beamsplitter and both sides of the compensator plates.

3.2 Beam paths at the combiner plates

In all cases, pairs of beams in the fringe tracking combiner will interfere at a 50% beam combiner plate. The trajectories of a typical pair of right- and left-ward propagating beams towards and through such a plate are shown in Figure 4. Note that the reflected left hand side (LHS) beam passes through the AR coating twice, while all other beams only traverse the coating once. It is desirable that the intensities of the two emergent beams (RR/LT and RT/LR) be equal otherwise there will be a loss in apparent fringe contrast leading to a lowering of signal-to-noise.

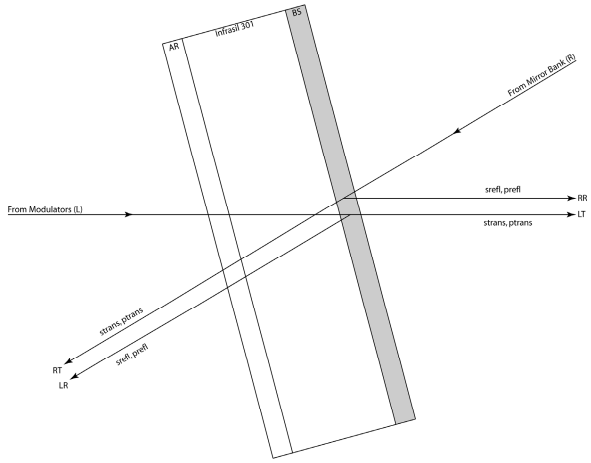

Fig.4. Representative diagram of the 50% beamsplitter combination point. There are 2 outputs after beam combination: right reflected (RR), left transmitted (LT) and right transmitted (RT), left reflected (LR).

4. VISIBILITY FACTORS

In this paper three factors were investigated that can serve to reduce the fringe visibility, and as a result the beam combiner signal-to-noise. These are:

(a) The presence of unequal beam intensities at the beamsplitter plates.
(b) Phase differences in the interferences arising from the orthogonal s and p states.
(c) Group delay effects when passing though the multi-layer dielectric coatings.

The next three subsections calculate these three factors respectively for each of the FT combination paths: A-B, C-B, F-B, D-E, C-G, and C-H.

4.1 Intensity mismatch

Intensity mismatch can arise due to unequal reflection and transmission factors within the beam combiner or the inability of optics to perfectly relay beams and superimpose them at combination.

To calculate intensity mismatch the total throughput in s and p were calculated for both the reflected and transmitted intensities of each beam (I_{refl} and I_{trans}). Taking the ratio of reflected and transmitted intensities, $\rho = I_{refl}/I_{trans}$, the visibility loss factor due to intensity mismatch is given by equation (1).[5]

$$I_{refl} = I_{1(path1)} * I_{2(path1)} * I_{3(path1)} * \ldots$$
$$I_{trans} = I_{1(path2)} * I_{2(path2)} * I_{3(path2)} * \ldots$$
$$\rho = I_{refl} \Big/ I_{trans}$$
$$V_{mismatch} = \frac{2}{\rho^{1/2} + \rho^{-1/2}} \qquad (1)$$

Some paths are very symmetric, such as path C-B, which leads to an insignificant reduction in fringe contrast. Path C-B's RR/LT output is perfectly symmetric and therefore, for perfectly manufactured coatings there is no visibility loss, as can be seen in Figures 5, 6 and 7. Other paths are less symmetric, especially those paths incorporating a compensator plate or a 33.33% beamsplitter; these paths show greater visibility losses. Typical visibility losses range between 0% in the best case and 8% in the worst case.

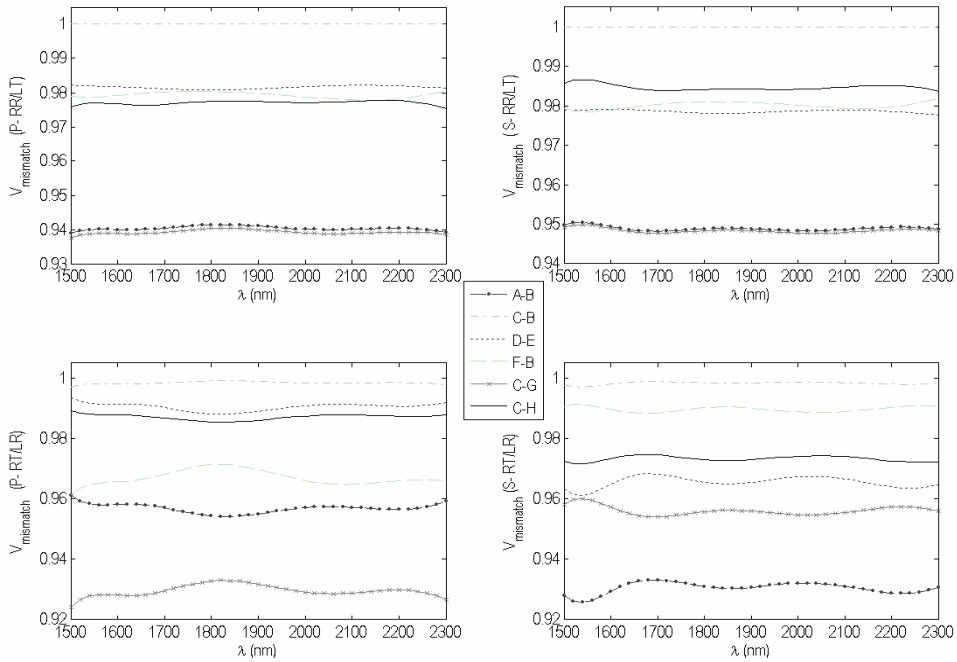

Fig.5. The above plots show the visibility loss factors for each combination path as a function of wavelength due to intensity mismatch. The four graphs show the two combiner outputs with two respective polarizations (s and p). These factors were calculated using equation (1). Paths showing the lowest visibility losses are very symmetric with insignificant reduction in fringe contrast. Other less symmetric paths, such as paths with compensator plates or a 33.33% beamsplitter, show higher visibility losses. Visibility losses range from 0% to 8% in the worst case.

4.2 Polarization

Optimally two beams would undergo the same sequence of reflections and transmissions through the beam combiner, experiencing equal phase shifts and producing two independent but identical fringes in s and p. However, this symmetry is not always possible and thus effects on fringe visibility ensue. The losses in visibility due to polarization effects are therefore caused by the interference patterns of the s and p polarization states being slightly offset from one another at the detector.

Visibility loss factors due to polarization can be calculated by initially summing the phase after each coating interaction in the s and p polarization states (ϕ_s,ϕ_p) from this the polarization difference, ϕ_{sp}, can be found by taking the difference, $\phi_{sp}=\phi_s-\phi_p$. Finally, equation (2)[6] can be used to derive the visibility loss factors due to polarization. These effects have proven to be very small for the MROI coatings and beam combiner architecture, <1.0% for all combination paths, as plotted in Figure 6.

$$\phi_s = \sum \phi_{s1} + \phi_{s2} + \phi_{s3} + \ldots$$
$$\phi_p = \sum \phi_{p1} + \phi_{p2} + \phi_{p3} + \ldots$$
$$\phi_{sp} = \phi_s - \phi_p$$
$$V_{pol} = \left| \cos\left(\frac{\phi_{sp}}{2} \right) \right| \qquad (2)$$

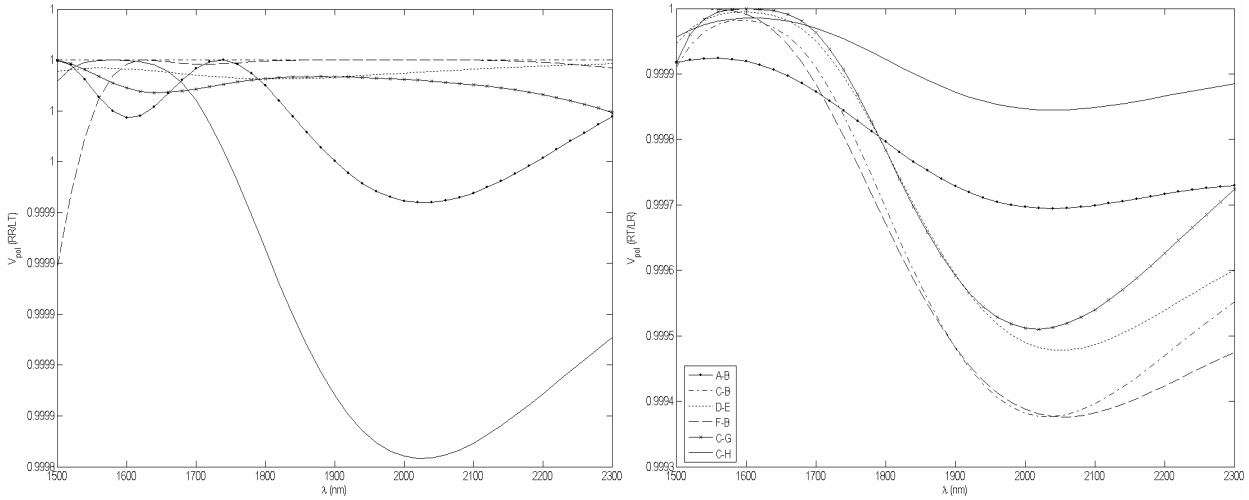

Fig.6. The above plots show the visibility factors due to polarization differences between s and p versus wavelength. The two plots correspond to the two combiner outputs (left) RR/LT and (right) RT/LR.

4.3 Group delay

The group delay is proportional to the rate of change of phase as a function of wave number evaluated at the center of the bandpass (in this case a particular spectral channel within the H or K band). If the group delay across the bandpass is not flat, then in principle, fringes at different wavelengths within the bandpass will be slightly offset in phase. The detector measures the sum of these fringes; hence, the phase offsets will lead to a reduction in the polychromatic fringe visibility. The magnitude of this effect was computed using equation (3), where a spectral resolution of R=30 was assumed and hence coherence lengths (for the central spectral channel in the H and K bands) of Λ_{coh}= 49.5μm and Λ_{coh}=64.5μm respectively.

Overall, these visibility loss factors were small (less than or equal to 1%) for all combination paths (Figure 7), indicating the value of utilizing the predicted group delay as a metric when optimizing the coating designs.

$$\delta_{sGD} = \sum \delta_{sGD1} + \delta_{sGD2} + \delta_{sGD3} + \ldots$$
$$\delta_{pGD} = \sum \delta_{pGD1} + \delta_{pGD2} + \delta_{pGD3} + \ldots$$
$$\delta_{GD} = \delta_{sGD} - \delta_{pGD}$$
$$V_{GD} = \frac{\sin\left[\pi \frac{\delta_{GD}}{\Lambda_{coh}}\right]}{\pi \frac{\delta_{GD}}{\Lambda_{coh}}} \qquad (3)$$

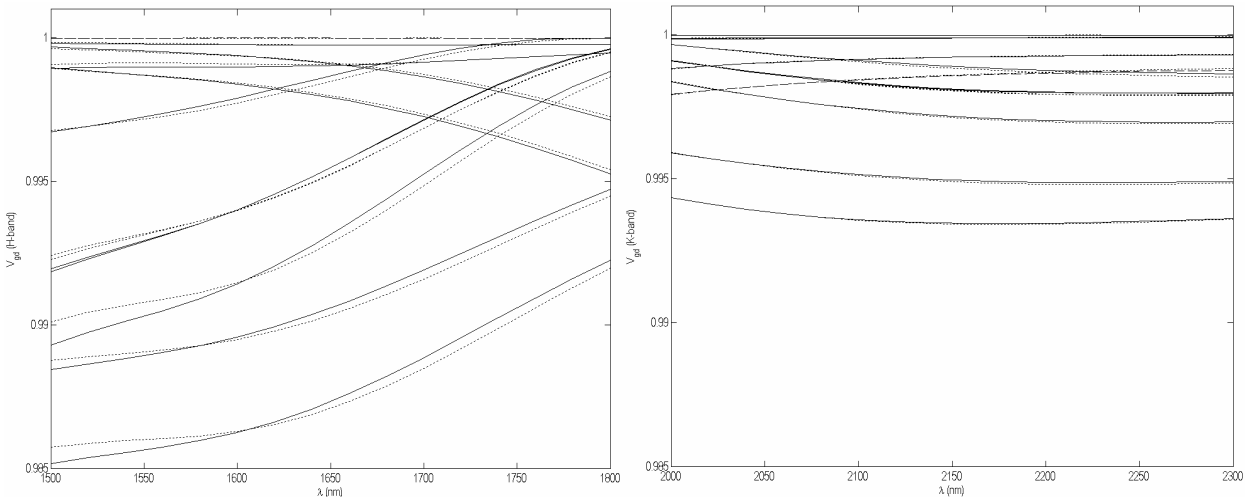

Fig.7. The above plots show trends in the group delay visibility factors for all paths, polarizations, and outputs for (left) H-band and (right) K_s-band. Dotted lines represent the s-polarization states and solid lines represent p-polarization states.

5. COATING PERFORMANCE: THEORETICAL VS. IDEAL

A useful way of assessing the performance of the coating designs is to normalize the measured visibilities with those that would arise if "perfect" coatings had been used, i.e. beamsplitter coatings with wavelength independent 50:50 or 33.33:66.67 splitting ratio, and AR coatings with 0 reflectivity, and with uniform group delay across all bandpasses. The value of this is that it removes the effect of the beam combiner architecture which though important, is not the focus here.

Figure 7 shows the normalized visibility loss factors, V/V_{ideal}, for all combination paths and outputs (RR/LT and RT/LR). Results show that the performance of the three coatings within the combiner is excellent with visibility losses comparable to that of the combiner implementing perfect coatings. In some cases performance of the actual coatings are superior to that of the perfect coatings which is a result of architectural limitations as well as intensity mismatch being less with the actual coatings than for the perfect case, e.g. perfect reflections of 50% followed by 33% give an intensity difference of 50%-33%=17% whereas actual coatings, say 49% and 34% reflections, give a smaller intensity difference (15%) yielding a smaller intensity mismatch and greater visibility.

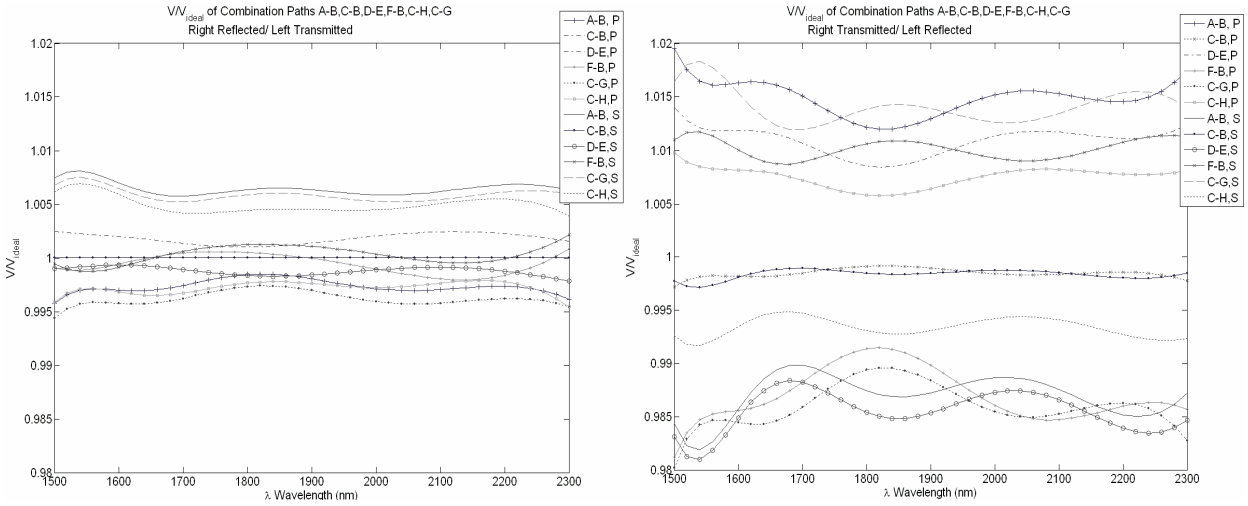

Fig.8. Above are plots showing the calculated visibility due to intensity mismatch (V) normalized by the visibility assuming perfect coatings (V_{ideal}) for (left) RR/LT and (right) RT/LR.

PATH	Wavelength (λ)		V	V_{ideal}	V/V_{ideal}	VI
A-B	Ks	1640	0.940	0.943	0.997	0.701
	H	2140	0.940	0.943	0.997	0.703
C-B	Ks	1640	1.000	1.000	1.000	0.492
	H	2140	1.000	1.000	1.000	0.493
D-E	Ks	1640	0.982	0.980	1.002	0.403
	H	2140	0.982	0.980	1.002	0.406
F-B	Ks	1640	0.980	0.980	1.000	0.401
	H	2140	0.978	0.980	0.998	0.398
C-G	Ks	1640	0.939	0.943	0.996	0.677
	H	2140	0.939	0.943	0.996	0.681
C-H	Ks	1640	0.976	0.980	0.997	0.395
	H	2140	0.978	0.980	0.998	0.398

PATH	Wavelength (λ)		V	V_{ideal}	V/V_{ideal}	VI
A-B	Ks	1640	0.949	0.943	1.006	0.682
	H	2140	0.949	0.943	1.006	0.683
C-B	Ks	1640	1.000	1.000	1.000	0.491
	H	2140	1.000	1.000	1.000	0.493
D-E	Ks	1640	0.979	0.980	0.999	0.396
	H	2140	0.979	0.980	0.999	0.398
F-B	Ks	1640	0.980	0.980	1.000	0.401
	H	2140	0.979	0.980	1.000	0.401
C-G	Ks	1640	0.948	0.943	1.006	0.709
	H	2140	0.948	0.943	1.006	0.713
C-H	Ks	1640	0.985	0.980	1.005	0.412
	H	2140	0.985	0.980	1.005	0.414

PATH	Wavelength (λ)		V	V_{ideal}	V/V_{ideal}	VI
A-B	Ks	1640	0.958	0.943	1.016	0.699
	H	2140	0.957	0.943	1.015	0.701
C-B	Ks	1640	0.998	1.000	0.998	0.490
	H	2140	0.998	1.000	0.998	0.492
D-E	Ks	1640	0.991	0.980	1.012	0.401
	H	2140	0.991	0.980	1.011	0.405
F-B	Ks	1640	0.966	0.980	0.986	0.400
	H	2140	0.965	0.980	0.985	0.398
C-G	Ks	1640	0.928	0.943	0.984	0.682
	H	2140	0.929	0.943	0.986	0.685
C-H	Ks	1640	0.988	0.980	1.008	0.394
	H	2140	0.988	0.980	1.008	0.397

PATH	Wavelength (λ)		V	V_{ideal}	V/V_{ideal}	VI
A-B	Ks	1640	0.932	0.943	0.989	0.679
	H	2140	0.930	0.943	0.986	0.681
C-B	Ks	1640	0.999	1.000	0.999	0.489
	H	2140	0.998	1.000	0.998	0.491
D-E	Ks	1640	0.967	0.980	0.987	0.395
	H	2140	0.966	0.980	0.986	0.397
F-B	Ks	1640	0.989	0.980	1.009	0.399
	H	2140	0.989	0.980	1.010	0.400
C-G	Ks	1640	0.955	0.943	1.013	0.700
	H	2140	0.956	0.943	1.014	0.704
C-H	Ks	1640	0.974	0.980	0.995	0.410
	H	2140	0.973	0.980	0.994	0.413

Table.1. The above tables show the visibility (V), ideal visibility (V_{ideal}), visibility*intensity (VI), and visibility normalized by the ideal (V/V_{ideal}). From left to right: p-polarization and combiner output RR/LT**,** s-polarization and combiner output RR/LT, p-polarization and combiner output RT/LR, and s-polarization and combiner output RT/LR.

Visibility loss factors due to intensity mismatch, V, as well as visibility loss factors for "perfect" coatings (V_{ideal}) are calculated and summarized in Tables 1-4 for each combination path through the FT beam combiner. These values are given for the central spectral channel in the H and K_s bands (2140nm and 1640nm respectively). V and V_{ideal} are then normalized to show the overall performance of the coatings within the combiner (V/V_{ideal}). The last column gives the computed visibility loss factor times the intensity at the respective output, VI, which gives an estimation of the variation

in signal-to-noise (S/N) at each output (since in the readout noise dominated regime, the S/N scales as a power of VI). In most cases the S/N is not equal at all outputs, which is primarily a result of the geometry of the beam combiner itself. In conclusion it was found that all three coatings lead to a typical visibility loss of only 1% through the combiner.

6. CONCLUSIONS

Overall the performance of the three custom coatings is excellent. The analysis showed that the greatest visibility losses arise from intensity mismatch which is most effected by combination path asymmetries (i.e. the most symmetric paths result in the highest visibilities). The losses due to polarization and group delay are minimal, less than or equal to 1%, for all the coatings and combination paths. Cumulatively, the theoretical visibility losses are $\leq 6\%$ in all cases for reflections and transmissions through the coatings as well as for combiner architecture. From the analysis it has been determined that the coatings will not be a limiting factor in the performance of the FT beam combiner and meet the MROI top level science goals. All three coatings are awaiting application by *Optical Surface Technologies* in Albuquerque, New Mexico and the construction of the MROI fringe tracker will commence this fall.

ACKNOWLEDGEMENTS

The Magdalena Ridge Observatory (MRO) is funded by Agreement No. N00173-01-2-C902 with the Naval Research Laboratory (NRL). MRO Interferometer is hosted by the New Mexico Institute of Mining and Technology (NMT) at Socorro, NM, USA, in collaboration with the University of Cambridge (UK).

REFERENCES

[1] M.J. Creech-Eakman, et.al, "Magdalena Ridge Observatory interferometer: progress towards first light," in *Optical and Infrared Interferometry. Edited by Markus Schöller, William C. Danchi, and Francoise Delplancke. Proc SPIE, Volume 7013 (2008).*

[2] C.A. Jurgenson, F.G. Santoro, F. Baron, A.M. Jorgensen, D.F. Buscher, M.J. Creech-Eakman, C.A. Haniff, J.S. Young, T.A. Coleman, K. M. McCord, E.K. Block, "Fringe tracking at the MROI," in *Optical and Infrared Interferometry. Edited by Markus Schöller, William C. Danchi, and Francoise Delplancke. Proc SPIE, Volume 7013 (2008)*.

[3] J.T. Armstrong, D. Mozurkewich, T.A. Pauls, A.R. Haiian, "Bootstrapping the NPOI: keeping long baselines in phase by tracking fringes on short baselines," in *Astronomical Instrumentation. Edited by R.D. Reasenberg. Proc SPIE Vol 3350 (1998).*

[4] D. F. Buscher, E. J. Bakker, T. A. Coleman, M. J. Creech-Eakman, C. A. Haniff, C. A. Jurgenson, D. A. Klinglesmith III, C. B. Parameswariah, J. S. Young. "The Magdalena Ridge Observatory Interferometer: a high sensitivity imaging array," in *Unconventional Imaging II, Proc. SPIE 6307 (2006).*

[5] W. A. Traub. "Beam Combination and Fringe Measurement," in *Principles of Long Baseline Stellar Interferometry. Edited by Peter R. Lawson. Michelson Summer School (1999).*

[6] W. A. Traub, "Beam Combination and Fringe Measurement," in *Principles of Long Baseline Stellar Interferometry. Edited by Peter R. Lawson. Michelson Summer School (1999).*